Received: 28 April 2016 | Accepted: 14 August 2016

DOI: 10.1111/jace.14547

ORIGINAL ARTICLE

Journal of the American Ceramic Society

Empirical evidence for A-site order in perovskites

Kevin Tolman[1,a] | Rick Ubic[1,a] | Bing Liu[2] | Izaak Williamson[1,a] | Katherine Bedke[1] | Eric B. Nelson[1,a] | Lan Li[1,3,a] | Xiang Ming Chen[3,a]

[1]Micron School of Materials Science and Engineering, Boise State University, Boise, Idaho

[2]Laboratory of Dielectric Materials, School of Materials Science & Engineering, Zhejiang University, Hangzhou, China

[3]Center for Advanced Energy Studies, Idaho Falls, Idaho

Correspondence
Kevin Tolman, Micron School of Materials Science and Engineering, Boise State University, Boise, Idaho.
Email: kevintolman@boisestate.edu

Funding information
National Science Foundation, Grant/Award Number: DMR-1052788;

Abstract

Models for composition-structure relationships are useful in both the lab and industry, yet few exist for perovskites-containing extrinsic defects or cation ordering. In this work, an empirical model is used to predict the existence of A-site cation ordering. Specifically, four compositions in the $Na_{(1-3x)/2}La_{(1+x)/2}TiO_3$ system (x=0.0, 0.0533, 0.1733 and 0.225) were synthesized using a conventional solid-state mixed-oxide method. The structure of the x=0 end-member ($Na_{0.5}La_{0.5}TiO_3$) has been reported in various space groups, but always with a random distribution of Na^+ and La^{3+} on the A site; however, empirical modeling suggests that it is not only ordered but also that a small volume increase accompanies the ordering process. While no evidence of long-range A-site ordering is observed in this composition via X-ray or neutron diffraction, electron-diffraction data indicate short-range ordering of Na^+ and La^{3+} ions, with the degree of cation ordering decreasing (but the scale of ordered domains and degree of vacancy ordering generally increasing) with increasing x. First-principles calculations via density functional theory support both conclusions that short-range ordering in $Na_{0.5}La_{0.5}TiO_3$ is stable and that it results in a volume increase with respect to the disordered analog. A similar analysis has been conducted for the $Li_{(1-3x)/2}La_{(1+x)/2}TiO_3$ and $Na_{(1-3x)/2}La_{(1+x)/2}(Mg_{0.5}W_{0.5})O_3$ solid solutions. These systems provide additional validation of the accuracy and versatility of the empirical modeling method used.

KEYWORDS
modeling/model, perovskites, vacancies

1 | INTRODUCTION

Predicting perovskite structures is a subject of continuous and significant interest. Perovskites arguably exhibit a wider variety of useful phenomena (eg, ferroelectricity, piezoelectricity, superconductivity, colossal magnetoresistance, etc.) than any other structure type.[1] Predicting structures—and, by extension, properties—based on chemical compositions, without the need for expensive trial and error or time-consuming computation, is the primary key to fully exploiting these highly useful materials.

The compound $Na_{0.5}La_{0.5}TiO_3$ is the x=0 end-member of the $Na_{(1-3x)/2}La_{(1+x)/2}TiO_3$ (NLT) solid solution and belongs to the loparite family of minerals found in foidolites and aegirine-albite metasomatic rocks. It is particularly remarkable because it exhibits quantum paraelectricity at low temperatures (<50 K).[2] Furthermore, it is thought that the paraelectric phase at these low temperatures is stabilized by "zero point quantum fluctuations" which prevent the freezing of its ferroelectric soft mode.[3]

[a]Member, The American Ceramic Society.

Evidence of short-range A-site cation and vacancy ordering domains is difficult to establish via X-ray diffraction (XRD); however, electron diffraction is generally more sensitive to such structural effects. Short-range A-site cation ordering of the type 1:1 can be inferred by the existence of diffuse pseudocubic ½{even,even,odd} β superlattice reflections.

All previous investigations of $Na_{0.5}La_{0.5}TiO_3$ have reported a disordered long-range distribution of the A-site cations (ie, random distributions of Na^+ and La^{3+} cations). The first such studies[4-6] reported that the structure of $Na_{0.5}La_{0.5}TiO_3$ was cubic, space group $Pm\bar{3}m$. Others later proposed an orthorhombic structure in space group *Pnma*.[7-9] Most recently, several groups[10-16] have used synchrotron- and neutron-diffraction data to establish either tetragonal (*I4/mcm*) or trigonal ($R\bar{3}c$) structural models, with a phase transition to an orthorhombic form in the region $0<x<0.05$. Knapp & Woodward[13] suggested that the A-site ordering observed in the analogous perovskite $(Na_{0.5}La_{0.5})(Mg_{0.5}W_{0.5})O_3$ would imply that $Na_{0.5}La_{0.5}TiO_3$ should also have A-site cation ordering; however, they observed no such long-range ordering. Garcia-Martin et al.[17] used electron diffraction to observe diffuse ½{even,even,odd} β superlattice reflections in $Na_{0.5}La_{0.5}TiO_3$, which they attributed to ordered nanodomains (ie, short-range order).

Ruiz et al.[8] initially studied the structures of $Na_{0.42}La_{0.5267}TiO_3$ (x=0.05) and $Na_{0.24}La_{0.5867}TiO_3$ (x=0.17) by electron and neutron diffraction as a means to determine the structures between the two end members, $Na_{0.5}La_{0.5}TiO_3$ (x=0) and $La_{2/3}TiO_3$ (x=⅓). They found that more than one type of superlattice reflection existed for these compositions and proposed orthorhombic (*Ibmm*) structures for both, each containing small octahedral tilt angles. Ruiz et al.[9] later studied these compositions again plus $Na_{0.165}La_{0.6117}TiO_3$ via electron and neutron diffraction to re-address the superlattice reflections, and they claimed that the ½{even,even,odd} reflections were formed by three sets of micro-domains; however, their Rietveld refinement fit for x=0.17 was improved using *Pbmm* rather than *Ibmm*. They reported[8,9] an orthorhombic cell in space group *Pbmm* for x=0.05, *Ibmm* for x=0.17, and a doubled orthorhombic cell in *Cmmm* for x=0.225. In 2003, Howard and Zhang[18] proposed the *Cmmm* structure for $La_{2/3}TiO_3$ (x=⅓); however, Gönen et al.[19] found that $La_{2/3}TiO_3$ is isomorphous with the $Nd_{2/3}TiO_3$ model in *I4/mmm* reported by Richard et al.,[20] consisting of shifted $La_2Ti_3O_9$ slabs, yielding a $La_{2/3}TiO_3$ compound with a layered structure in which vacancies cluster on every third {001} plane.

While A-site ordering in perovskites is most commonly reported on pseudocubic {001} (layered), 1:1 A-site ordering can occur in two other geometries: {110} (columnar) and {111} (rock salt) (Figure 1). For example, (NaLa)$(MgW)O_6$ forms in tetragonal *P4/mmm* and orders with a layered geometry[21] while $(CaFe)Ti_2O_6$ forms in tetragonal $P4_2/nmc$ and orders with a columnar geometry,[22] and $(NaBa)(LiNi)F_6$ forms in cubic $Fm\bar{3}m$, ordering with a rock-salt geometry.[23] Other geometries are possible for different stoichiometries. For example, the 1:3 ordered $CaCu_3Ti_4O_{12}$ compound orders in a more complicated way in cubic space group $Im\bar{3}$.[24,25]

Inaguma et al.[14] refined the structure of $Na_{0.5}La_{0.5}TiO_3$ in both *I4/mcm* and $R\bar{3}c$ because the anti-phase octahedral tilting was difficult to quantify; however, they assumed a fully disordered structure. The octahedral tilting in *I4/mcm* is about a single pseudocubic axis parallel to the tetragonal c axis (ie, $a^0a^0c^-$ in Glazer's notation,[26]) whereas in $R\bar{3}c$ the degree of tilting is equal along all three pseudocubic <100> axes ($a^-a^-a^-$), which is equivalent to a tilt about the hexagonal c axis.

Using a combination of synchrotron and neutron powder diffraction data, Garg et al.[12] showed that $R\bar{3}c$ was a better description of the structure of $Na_{0.5}La_{0.5}TiO_3$ than *I4/mcm*. The octahedral tilting about the hexagonal [001] was quantified at about 8°. Again, no evidence of ordering was found; however, their synchrotron data did not extend below 5° (2θ) and they used a wavelength of 0.5 Å, which

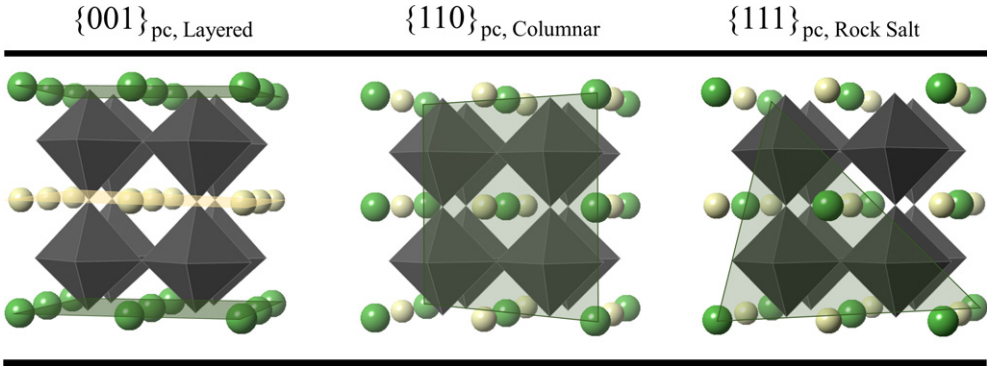

FIGURE 1 Pseudocubic view of $Na_{(1-3x)/2}La_{(1+x)/2}TiO_3$ for the three types of 1:1 geometries that A-site ordering can occur {001} (layered), {110} (columnar) and {111} (rock-salt) [Color figure can be viewed at wileyonlinelibrary.com]

means that the largest possible d spacing observable would have been 5.7 Å—far too small to detect a ½{001} superlattice peak at ~7.75 Å should one have existed. Similarly, they used a wavelength of 1.548 Å for their neutron-diffraction data, which did not extend below 20°; therefore, the maximum d spacing observable would have been just 4.5 Å. As a consequence, while higher-order superlattice reflections indicative of A-site order might have been detectable in these experiments, the stronger fundamental ½{001} peak could not have been detected even if present.

Superlattice ½{even,even,odd} β reflections observed by Garcia-Martin et al.[17] in electron-diffraction data suggested cation ordering in both $Na_{0.5}La_{0.5}TiO_3$ and $Na_{0.5}La_{0.5}ZrO_3$; however, the superlattice reflections of the former composition were much more diffuse. They hypothesized that short-range A-site ordering may form nanodomains in which the ordered planes are mutually perpendicular, as they would be on various pseudocubic {001}.

Recently, Ubic et al. studied $Sr_{1-3x}Ln_{2x}TiO_3$ (Ln=La, Nd, Ce)[27-29] and developed[30] a general empirical model for the effective sizes of A-site species (including vacancies) and anions in perovskites which can thus predict the pseudocubic lattice constants. By analyzing the systematic errors between the NLT experimental pseudocubic lattice constants $a_{pc,(Exptl.)}$ (Equation 1) and the predicted pseudocubic lattice constants (Equations 2-3) based on the empirical model, they suggested[30] the existence of A-site ordering in NLT, the degree of which decreased with increasing x; but they were unable to reconcile this conclusion with the reported structures of $Na_{0.5}La_{0.5}TiO_3$ or the counterintuitive apparent volume increase which the model predicted upon ordering in this system.

$$a_{pc,(Exptl.)} = \left(\frac{V}{Z}\right)^{1/3} \tag{1}$$

$$a'_{pc} = \sqrt{2}(r_A + r_X) \tag{2}$$

$$a''_{pc} = 2(r_B + r_X) \tag{3}$$

In Equations 1-3, V, Z, r_A, r_B, and r_X are the cell volume, number of ABX_3 units per unit cell, and the effective ionic radii of A, B, and X ions, respectively.[31]

The conventional tolerance factor[32] can be calculated as the ratio of

$$a'_{pc}/a''_{pc}$$

:

$$t = \frac{a'_{pc}}{a''_{pc}} = \frac{r_A + r_O}{\sqrt{2}(r_B + r_X)} \tag{4}$$

In 2007 Ubic et al.[33] published a method of calculating pseudocubic lattice constants and later[29-34] revised it in order to accommodate extrinsic defects, deriving from the revised formula a new model for tolerance factor:

$$t_1 = \frac{a_{pc} - 0.011730139}{0.7209203(r_B + r_X)} - 0.760998, \tag{5}$$

where r_B and r_X correspond to the published[31] ionic radii of B and X ions, respectively. Ideally t_1=t;[28,29] however, t_1 predicts tilt structures of perovskites better and does not require knowledge of r_A (but does require foreknowledge of a_{pc}). Equation 5 can also be solved for a_{pc} in terms of t_1, r_B, and r_X:

$$a_{pc} = 0.7209203(t_1 + 1.760998)(r_B + r_X) + 0.011730139 \tag{6}$$

Neither Equations 5 nor 6 requires explicit knowledge of the A-site size, which is a non-trivial problem especially when vacancies are involved. According to the model of Ubic et al.,[30] it is the sum of three separate terms: the ideal (Shannon) size, a bond-deformation (BD) term (Equation 7), and the effective size of vacancies, r_V (Equation 8):

$$BD = 7.4801 - 12.3139t_0 + 4.8257t_0^2 \tag{7}$$

$$r_V = -20.8983 + 36.9417t_0 - 14.1771t_0^2 \tag{8}$$

where t_0 corresponds to the conventional tolerance factor (Equation 4) for the x=0 composition. The effective anion size is reportedly[30] a function of t_1:

$$\frac{r_X}{r_X(id)} = 0.42983 + 0.56696t_1 \tag{9}$$

Finally, Ubic et al.[30] developed an empirical relation between t_1 and the conventional t, allowing the prediction of effective values for r_X without experimental a_{pc} data, thus their model can accurately predict a_{pc} values of A-deficient perovskites from published ionic radii data alone.

The present work provides both validation of this empirical model as well as confirmation of the true structure of several members of the $Na_{(1-3x)/2}La_{(1+x)/2}TiO_3$ solid solution. A total of four compositions (x=0, 0.0533, 0.1733 and 0.225) were synthesized and studied to investigate the sensitivity of this empirical model regarding short- and long-range A-site ordering.

The A site maintains a 2+ formal charge, which is conveniently formulated as:

$$Na_{\left(\frac{1-3x}{2}\right)}La_{\left(\frac{1+x}{2}\right)}V_xTiO_3$$

where V corresponds to vacancies. The defect chemistry can be formulated as:

$$La_2O_3 \overset{Na_{1/2}La_{1/2}TiO_3}{\rightarrow} 2La^{\bullet\bullet}_{Na} + 4V'_{Na} + 3O^x_O$$

There are three A-site components (ie, increasing [La], decreasing [Na], and increasing [V]) that must be

considered with this defect chemistry, and all are accounted for in this formulation.

The model as developed previously starts with the assumption of an "average" cation size $((1 - 3x)r_{Na} + (1 + x)r_{La})/4$ and the stoichiometry is purposely formulated so that x represents the degree of vacancy "doping" on this site (ie, x=[V]). Alternately, this system can be thought of as doping the "average" cation site with La^{3+} according to:

$$(Na_{1/2}La_{1/2})_{1-3x}La_{2x}TiO_3$$

In this way the model used here is exactly analogous to $A^{2+}{}_{(1-3x)}Ln^{3+}{}_{(2x)}BO_3$ systems already studied,[30] in which x=[V].

2 | MATERIALS AND METHODS

Four compositions in the system $Na_{(1-3x)/2}La_{(1+x)/2}TiO_3$ (x=0, 0.0533, 0.1733 and 0.225) were synthesized via the solid-state mixed-oxide route. No excess sodium was added to the compositions, but a sacrificial powder bed was used to induce a sodium-rich closed environment. Additionally, the calcination and sintering were conducted in a pre-contaminated crucible to inhibit sodium-loss into the crucible walls. As-received La_2O_3 (99.9%, Alfa-Aesar, Ward Hill, MA) powder was first hydroxylated by mixing with an excess of deionized water and drying overnight, forming $La(OH)_3$. Stoichiometric amounts of Na_2CO_3 (99.5%, Thermo Fisher Scientific Inc., Pittsburgh, PA), TiO_2 (99.9%, Aldrich Chemical Co., Milwaukee, WI), and $La(OH)_3$ were then ball-milled with yttria-stabilized ZrO_2 media using deionized water in a high-density nylon pot for ~24 hour. Powders were then dried overnight in an atmospheric drying oven at 80°C-100°C until the water was evaporated. Calcination was conducted at 1000°C for three hours in a box furnace (1807FL, CM Furnaces Inc., Bloomfield, NJ) with a sacrificial powder in an inverted pre-contaminated Al_2O_3 crucible placed on an Y_2O_3 plate. After calcination the powders were crushed using a mortar and pestle. Calcined powders were then sieved to under 250 μm and mixed in water with 2 wt% polyethylene glycol (PEG 10 000, Alfa-Aesar, Heysham, UK) powder which was dissolved in water prior to mixing. The mixture was then dried overnight in an atmospheric drying oven at 80°C-100°C until the water was evaporated. Cylindrical green compacts 8-10 mm in height and 10 mm in diameter were then formed by applying a uniaxial pressure of 63 MPa. Compacts were sintered for 3 hour at 1350°C with a sacrificial sodium-rich powder and the same pre-contaminated plate/inverted crucible apparatus previously described.

Powder XRD measurements were performed in a diffractometer (Miniflex-600, Rigaku, Woodlands, TX) operating with convergent-beam geometry and CuK_α radiation. Le Bail fits of the XRD data were analyzed using DiffracPLUS TOPAS 4.2 (Bruker AXS Inc., Madison, WI). The background was fitted with a fourth-order Chebychev polynomial, and asymmetry was corrected using the Finger et al. model.[35]

Scanning electron microscopy (S-3400N-II, Hitachi High-Technology, Tokyo, Japan) and quantitative energy dispersive X-ray spectroscopy (EDS) (Energy+, Oxford Instruments, UK) was performed on each of the samples to verify composition and homogeneity, as conventional processing can result in compositional fluctuations due to the volatility of sodium oxide. Quantitative EDS for each sample was performed using the same conditions (ie, accelerating voltage, beam current, and working distance). Amelia albite, lanthanum phosphate, and ilmenite standards were used to quantify Na, La, and Ti, respectively.

Specimens for transmission electron microscopy (TEM) (JEM-2100 HR, JEOL, Japan) were prepared from sintered pellets by mechanically cutting them with a diamond wafering blade then polishing the faces via conventional ceramographic techniques, finishing with a precision ion polisher (Model 691 PIPS, Gatan, Pleasanton, CA) at low ion-beam angles to achieve electron transparency (ie, thickness ~100 nm). Amorphous material cuased by ion damage was removed using a plasma cleaner (Model 1400, E. A. Fischione Instruments Inc., Export, PA) prior to observation in the TEM.

The Vienna Ab initio Software Package[36] was used to conduct structural and energetic calculations according to density functional theory (DFT). The spin-polarized generalized gradient approximation was used within the Perdew Burke Ernzerhoff formalism.[37] Plane-wave basis sets were expanded using projector-augmented wave[38,39] pseudopotentials to a cutoff energy of 500 eV. The Brillouin zone integration was performed on a 10 × 10 × 10 gamma-centered mesh for tetragonal and a 10 × 10 × 5 gamma-centered mesh for trigonal settings. To account for Fermi surface broadening, a Gaussian smearing value of 0.05 eV was applied. All relaxations of the lattice parameters and atomic positions were performed until residual forces were reduced to 0.01 eV/Å.

3 | RESULTS AND DISCUSSION

No secondary phases were detected in $Na_{(1-3x)/2}La_{(1+x)/2}TiO_3$ samples via XRD (Figure 2) or EDS (Table 1); however, no ordering superlattice reflections were observed via XRD in $Na_{0.5}La_{0.5}TiO_3$ either. The lack of superlattice reflections was expected, as the ordering reportedly exists[17]

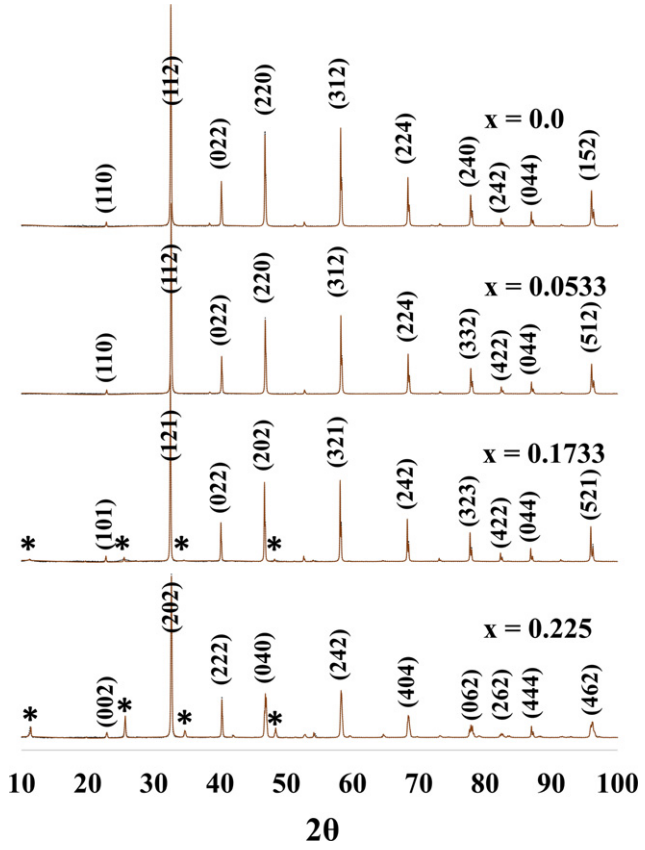

FIGURE 2 $Na_{(1-3x)/2}La_{(1+x)/2}TiO_3$ X-ray diffraction x=0.0-0.225. Peaks marked with * result from long-range A-site cation ordering [Color figure can be viewed at wileyonlinelibrary.com]

TABLE 1 $Na_{(1-3x)/2}La_{(1+x)/2}TiO_3$ energy dispersive X-ray spectroscopy (EDS) results. Both ideal and experimentally determined stoichiometries are shown

Nominal composition	x (ideal)	Na	La	x (Exptl.)
$Na_{0.5}La_{0.5}TiO_3$	0	0.4957 (27)	0.5015 (14)	0.0000 (29)
$Na_{0.42}La_{0.5267}TiO_3$	0.0533	0.4187 (33)	0.5271 (11)	0.0542 (33)
$Na_{0.24}La_{0.5867}TiO_3$	0.1733	0.2389 (54)	0.5871 (20)	0.1741 (98)
$Na_{0.1625}La_{0.6125}TiO_3$	0.2250	0.1607 (62)	0.6131 (21)	0.2262 (42)

as nanodomains within a disordered matrix. No long-range order exists. The XRD patterns have been indexed in the following space groups: x=0 in *I*4/*mcm*, x=0.0533 in *Ibmm*, x=0.1733 in *Pmma*, and x=0.225 in *Cmmm* (Figure 2).

Figure 3 shows a comparison of calculated XRD patterns for the x=0.1733 composition in space group *Pmma*. In this setting the A-site Wyckoff positions are $2e(\frac{1}{4},0,z)$ and $2f(\frac{1}{4},\frac{1}{2},z)$, each with a single degree of freedom. When z=0.75 on both 2*e* and 2*f*, the result is non-characteristic orbits in which the atomic positions are identical to those in an ideal perovskite. These z values were adjusted in model calculations to analyze their effects on XRD patterns. Four different combinations of z values were compared in both ordered and disordered variations of this composition. Figure 3 has been indexed according to the pseudocubic unit cell, which is related to the orthorhombic one in *Pmma* by the following matrix transformation:

$$[a_o b_o c_o] = \begin{bmatrix} 1 & 0 & -1 \\ 0 & 2 & 0 \\ 1 & 0 & 1 \end{bmatrix} \begin{bmatrix} a_{pc} \\ b_{pc} \\ c_{pc} \end{bmatrix}$$

Clearly, alterations in z correspond to A-site cation displacements along $[101]_{pc}$. The simulations show that the peaks at 11.39° and 25.69°, corresponding to β superlattice reflections ½(010) and ½(012), respectively, are due to cation ordering alone; whereas the peaks corresponding to A-site cation displacements were dependent on the nature of those displacements. Unequal 2*e* and 2*f* z parameters give rise to the ½(111) peak at 19.82° and contribute weakly to the ½(101) and ½(121) peaks at 16.17° and 28.16°, respectively. Equal 2*e* and 2*f* parameters yield strong ½(101) and ½(121) peaks but also contribute weakly to the ½(111) peak.

EDS results are shown in Table 1 and demonstrate that there were no impurities detected and that the overall compositions were close (ie, within resolution error) to the nominal compositions. Moreover, the small amount of sodium loss was less than 0.68 at.% average absolute relative error.

It is well known that ordered structures generally pack more efficiently than disordered ones,[40] which is the basis for the decrease in specific volume generally observed upon crystallization, so ordering in complex perovskites is typically expected to result in a decrease in unit volume. Zhang et al.[41] reported pyrochlore-to-defect-fluorite results that support the conventional view of lattice contraction upon ordering. In that work, the lattice constant was found to decrease as Zr^{4+} (0.72 Å) was replaced by Sn^{+4} (0.69 Å). Part of the contraction is no doubt due to the size difference between these two species; however, the degree of order also reportedly increased (from defect-fluorite to pyrochlore) as the Sn^{4+} content (and so lattice constant) decreased. On the other hand, Karthik et al.[42] reported a decrease in cation order in lanthanide pyrohafnates as lattice constant decreased across the lanthanide series, which phenomenon was easily explainable due to the large size reduction in the lanthanide species from La^{3+} to Lu^{3+}. In the case of B-site ordered $Ba(Mg_{1/3}Ta_{2/3})O_3$, Mani et al.[43] reported a unit cell with a_{pc}=4.0868 Å. In this case, the modeling technique described above results in unexpectedly large positive errors in both a'_{pc} (0.952%) and a''_{pc} (1.595%), suggesting an overestimation of r_B caused by the volume shrinkage induced by ordering. Other examples are listed in Tables 2 and 3. Table 2 shows the results using the weighted average of B-site cation sizes[31] while r_B values in Table 3[43-48] have been reduced, effectively

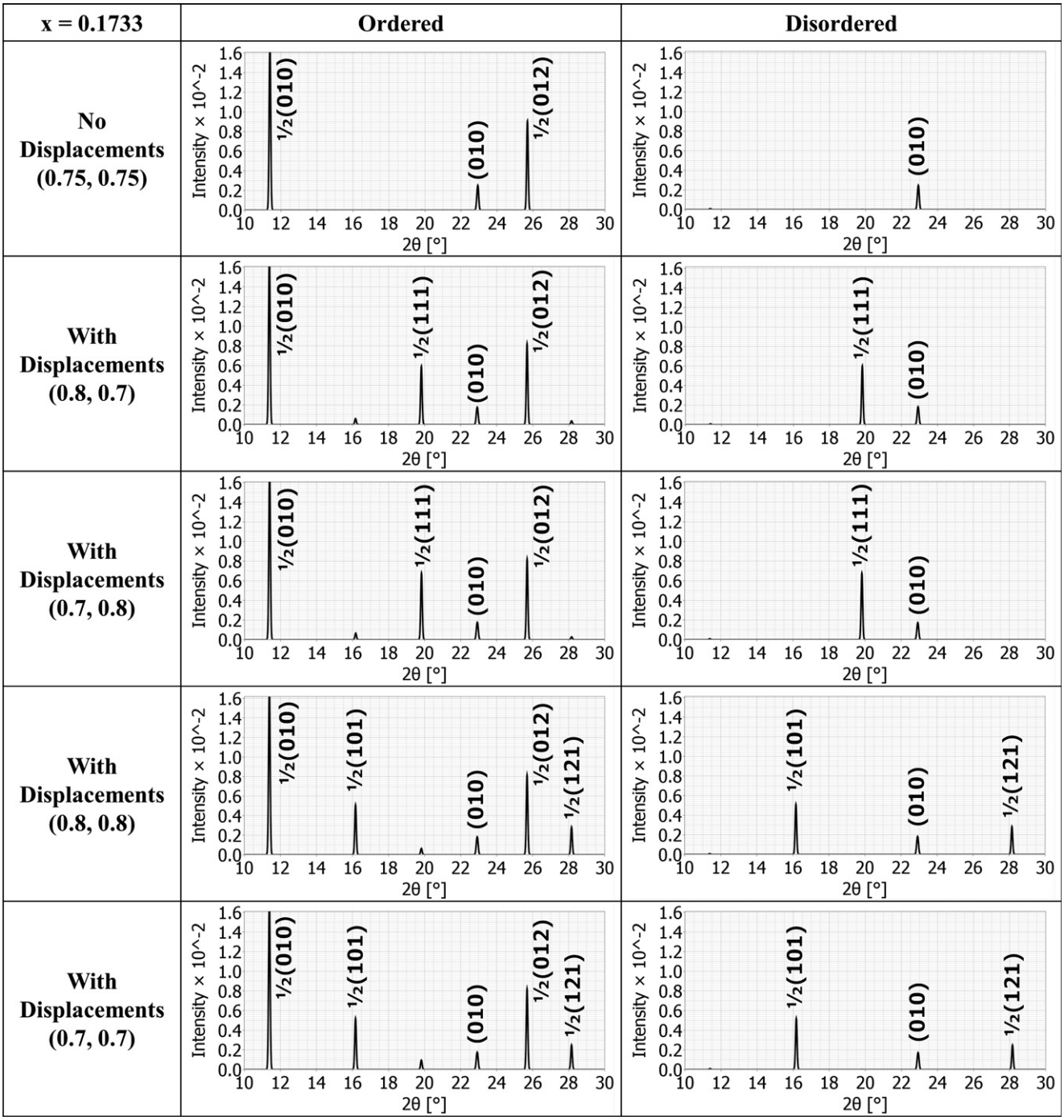

FIGURE 3 Simulated XRD traces for $Na_{(1-3x)/2}La_{(1+x)/2}TiO_3$ x=0.1733 in *Pmma*, varying both the ordering state and A-site atomic positional displacements. The peaks have been indexed according to the pseudocubic unit cell

decreasing the absolute errors in both a'_{pc} (0.000%) and a''_{pc} (0.000%). In order to validate the assumption of volume shrinkage upon B-site ordering and thereby validate this method, the effect of B-site ordering was also calculated via DFT for $La(Zn_{0.5}Ti_{0.5})O_3$, reported[44] to form with B-site ordering in space group $P2_1/n$. These calculations show that the unit volume does, in fact, decrease upon ordering. The disordered form had a calculated unit volume of 253.27 Å^3 compared to the ordered variant which had a unit volume of 252.24 Å^3.

The same volume shrinkage observed on B-site ordering might be assumed for the case of A-site ordering as well; however, it seems that the volume actually increases for A-site ordering (Tables 4-9). First-principles DFT calculations for $Na_{0.5}La_{0.5}TiO_3$ in a tetragonal setting (*I4/mcm*) show that the unit volume actually increases upon A-site layered

TABLE 2 B-site ordered compounds using ideal B cation sizes

Composition	$a_{pc(exptl)}$ (Å) Equation (1)	a_{pc} (Å) Equation (6)	Error (%)	a'_{pc} (Å) Equation (2)	Error (%)	a''_{pc} (Å) Equation (3)	Error (%)
$Ba(Mg_{1/3}Ta_{2/3})O_3$[a]	4.0868	4.1467	1.47	4.1257	0.95	4.1519	1.59
$La(Zn_{1/2}Ti_{1/2})O_3$[b]	3.9503	3.9903	1.01	3.9966	1.17	3.9868	0.92
$Ca(Mg_{1/2}W_{1/2})O_3$[c]	3.8707	3.9515	2.09	3.9628	2.38	3.9468	1.97
$Sr(Mg_{1/2}W_{1/2})O_6$[d]	3.9530	4.0298	1.94	4.0129	1.52	4.0295	1.94
$Ba(Mg_{1/2}W_{1/2})O_3$[e]	4.0542	4.1339	1.97	4.1152	1.51	4.1395	2.10
$Pb(Mg_{1/2}W_{1/2})O_3$[f]	4.0085	4.0724	1.60	4.0469	0.96	4.0746	1.65

[a]Ref. [40].
[b]Ref. [41].
[c]Ref. [42].
[d]Ref. [43].
[e]Ref. [44].
[f]Ref. [45].

TABLE 3 B-site ordered compounds accounting for the effect of B-site ordering

Composition	$r_{B\ Corr.}$ (Å)	a_{pc} (Å) Equation (6)	Error (%)	a'_{pc} (Å) Equation (2)	Error (%)	a''_{pc} (Å) Equation (3)	Error (%)
$Ba_3MgTa_2O_9$[a]	−0.028 35	4.0806	−0.15	4.0868	0.00	4.0868	0.00
La_2ZnTiO_6[b]	−0.027 21	3.9536	0.08	3.9504	0.00	3.9503	0.00
Ca_2MgWO_6[c]	−0.053 85	3.8750	0.11	3.8707	0.00	3.8707	0.00
Sr_2MgWO_6[d]	−0.105 47	3.9395	−0.34	3.9530	0.00	3.9530	0.00
Ba_2MgWO_6[e]	−0.042 39	4.0464	−0.19	4.0542	0.00	4.0542	0.00
Pb_2MgWO_6[f]	−0.071 26	3.9982	−0.26	4.0085	0.00	4.0085	0.00

[a]Ref. [40].
[b]Ref. [41].
[c]Ref. [42].
[d]Ref. [43].
[e]Ref. [44].
[f]Ref. [45].

TABLE 4 Density functional theory (500 eV) tetragonal $Na_{0.5}La_{0.5}TiO_3$ A-Site ordered nanodomain structures

Tetragonal	*a* (Å)	*b* (Å)	*c* (Å)	V (Å^3)
Columnar	5.4901	5.4901	7.8880	237.75
Layered	5.4744	5.4744	7.9358	237.83
Rocksalt	5.4660	5.4660	7.8901	235.74
Disordered	5.5187	5.5187	7.7838	237.06

TABLE 5 Density functional theory (500 eV) trigonal $Na_{0.5}La_{0.5}TiO_3$ A-Site ordered nanodomain structures

Hexagonal	*a* (Å)	*b* (Å)	*c* (Å)	V (Å^3)
Columnar	5.5356	5.5356	13.5601	359.82
Layered	5.5304	5.5304	13.5573	359.70
Rocksalt	5.5274	5.5274	13.5256	357.87
Disordered	5.5185	5.5185	13.5080	356.31

or columnar type ordering compared to the disordered structure (Table 4); which is both counterintuitive and opposite to the shrinkage observed upon B-site ordering. The relative energy results suggested that the type of A-site ordering in NLT would likely be layered, as expected. These calculations included only a few unit cells and so the results are consistent with the existence of ordered nanodomains found experimentally via electron diffraction and do not necessarily imply the existence of long-range order.

The same DFT calculations for $Na_{0.5}La_{0.5}TiO_3$ in a hexagonal setting show that the unit volume increases upon any type of A-site ordering (Table 5); however, once again the layered type ordering is the most energetically favorable geometry. Table 6 shows the calculated errors corresponding to the empirical model of Ubic et al.[30] This model shows a small but negative error in a'_{pc} for the x=0 composition which suggests that the calculated a'_{pc} (which is a function of the A–O bond length, Equation 2), which assumes cation disorder, is smaller than the $a_{pc\ (Exptl.)}$. The difference can be explained if the A-site-ordered form, suggested to exist in nanodomains, has a larger unit volume than does the disordered form. Errors generally increase as

TABLE 6 $Na_{(1-3x)/2}La_{(1+x)/2}TiO_3$ calculated pseudocubic lattice constants a'_{pc} and a''_{pc}

Composition	a (Å)	b (Å)	c (Å)	a_{pc}	a'_{pc}	Error%	a''_{pc}	Error%
x=0.0[a]	5.4769	5.4769	7.7539	3.8742	3.8670	−0.19	3.8663	−0.20
x=0.0533[b]	5.4798	5.4753	7.7432	3.8727	3.8677	−0.13	3.8626	−0.26
x=0.1733[b]	5.4763	7.7624	5.4766	3.8754	3.8860	0.28	3.8782	0.07
x=0.2233[b]	7.7234	7.7485	7.7803	3.8753	3.9011	0.66	3.8950	0.51
x=0.3333[c]	3.8565	3.8565	24.645	3.9384	3.9467	0.21	3.9501	0.30

[a]Ref. [10].
[b]Ref. [9].
[c]Ref. [19].

TABLE 7 $Na_{(1-3x)/2}La_{(1+x)/2}TiO_3$ accounting for the cation effective sizes

Composition	$r_{A\ Corr.}$ (Å)	%	a_{pc}	Error%	a'_{pc}	Error%	a''_{pc}	Error%
x=0.0[a]	0.0251	1.183	3.8969	0.588	3.8706	−0.090	3.8776	0.090
x=0.0533[b]	0.0236	1.182	3.8873	0.377	3.8726	−0.001	3.8732	0.013
x=0.1733[b]	0.0052	0.460	3.8908	0.399	3.8754	0.001	3.8754	0.001
x=0.2233[b]	0.0005	0.047	3.9015	0.675	3.8881	0.330	3.8753	0.000
x=0.3333[c]	0.0000	0.000	3.9457	0.185	3.9449	0.165	3.9384	0.000

[a]Ref. [10].
[b]Ref. [9].
[c]Ref. [19].

TABLE 8 Density functional theory (500 eV) trigonal $Li_{0.5}La_{0.5}TiO_3$ A-Site ordered nanodomain structures

Hexagonal	a (Å)	b (Å)	c (Å)	V (Å^3)
Columnar	5.5221	5.5221	13.5280	357.33
Layered	5.5160	5.5160	13.5264	357.18
Rocksalt	5.5118	5.5118	13.5029	355.26
Disordered	5.5018	5.5018	13.5219	352.38

x increases (Table 6), suggesting that the degree of cation ordering simultaneously decreases. Structural models for $0<x\leq\frac{1}{3}$[9,19] show that the degree of cation ordering indeed decreases with x whilst the degree of vacancy ordering generally increases, and the $x=\frac{1}{3}$ end member ($La_{2/3}TiO_3$) has a layered structure in which slabs of $La_2Ti_3O_9$ are separated and sheared by interlayers without cations[19] (ie, full vacancy ordering). The empirical model, which just produces a 0.21% error for $La_{2/3}TiO_3$, is apparently sensitive to cation ordering (which affects bond lengths) but not vacancy ordering (which does not). It should be further noted that at x=0, where the strongest evidence of an ordering phenomenon exists, there can be no contribution from vacancy ordering. Even though thermodynamics dictates that a finite concentration of intrinsic vacancies exists even at x=0, there can be no 1:1 long-range vacancy ordering at this or other low-x compositions where the presence of vacancies is nonstoichiometric. Short-range ordering of vacancies at low-x compositions seems unlikely, particularly given the evidence from the $Na_{(1-3x)/2}La_{(1+x)/2}TiO_3$[9]

TABLE 9 $Na_{(1-3x)/2}La_{(1+x)/2}(Mg_{½}W_{½})O_3$ and $K_{(1-3x)/2}La_{(1+x)/2}(Mg_{½}W_{½})O_3$ summary results

Comp.	r_A (Å)	$r_{A\ (cor.)}$ (Å)	r_B (Å)	$r_{B\ (cor.)}$ (Å)	a' (Å)	$a'_{(Error)}$ (%)	a'' (Å)	$a''_{(Error)}$ (%)
NLMW[a]								
x=0	1.375	0.0058	0.660	−0.0268	3.9254	0.000	3.9254	0.000
x=0.1111	1.219	0.0133	0.660	−0.0266	3.9288	0.000	3.9288	0.000
x=0.2222	1.063	0.0041	0.660	−0.0417	3.9257	0.000	3.9257	0.000
KLMW[a]								
x=0	1.500	0.0735	0.660	−0.1048	3.9529	0.000	3.9529	0.00
x=0.1111	1.302	0.0552	0.660	−0.0821	3.9484	0.000	3.9484	0.000
x=0.2222	1.104	0.0257	0.660	−0.0698	3.940	0.000	3.940	0.000

[a]Ref. [46].

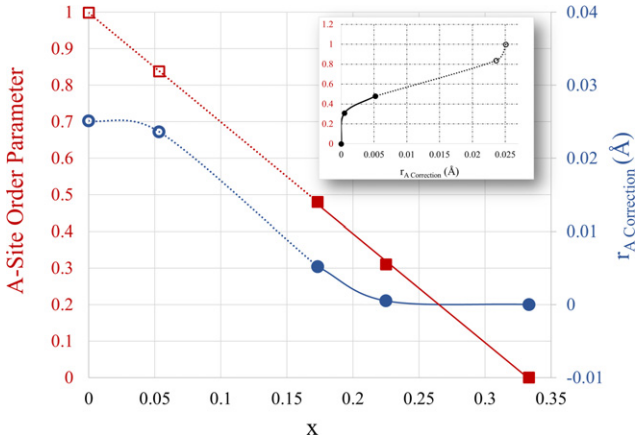

FIGURE 4 $Na_{(1-3x)/2}La_{(1+x)/2}TiO_3$ ordering from reported[9] site occupancies where the open data points are extrapolated according to the empirical model. Inset shows the order parameter as a function of $r_{A\ correction}$ (Å) and can be thought of as an empirical model for ordering (0=disorder, 1=fully ordered) [Color figure can be viewed at wileyonlinelibrary.com]

and $Li_{(1-3x)/2}La_{(1+x)/2}TiO_3$ systems,[49-60] which show that the degree of vacancy ordering increases and cation ordering decreases as x increases. Increasing the effective r_A value has the effect of both increasing a'_{pc} and, because of its effect on tolerance factor and hence r_O, a''_{pc}. Table 7 shows the results after increasing r_A in order to simultaneously minimize the absolute relative errors in both a'_{pc} and a''_{pc} in $0 \leq x \leq 0.055$ compositions.

If increasing r_A reduces the absolute error in a'_{pc}, then the initial underestimation in r_A could indicate A-site cation ordering (ie, such ordering manifests itself in this empirical model as an increased effective A-site size). Furthermore, the degree of this ordering can be calibrated from published models (Figure 4) and the model used to interpolate/extrapolate it for other compositions by comparing the error in a'_{pc} to that in either a''_{pc} or a_{pc}. In this case, the smaller correction needed at x=0.053 than at x=0 is indicative of the lower degree of order which one would anyway

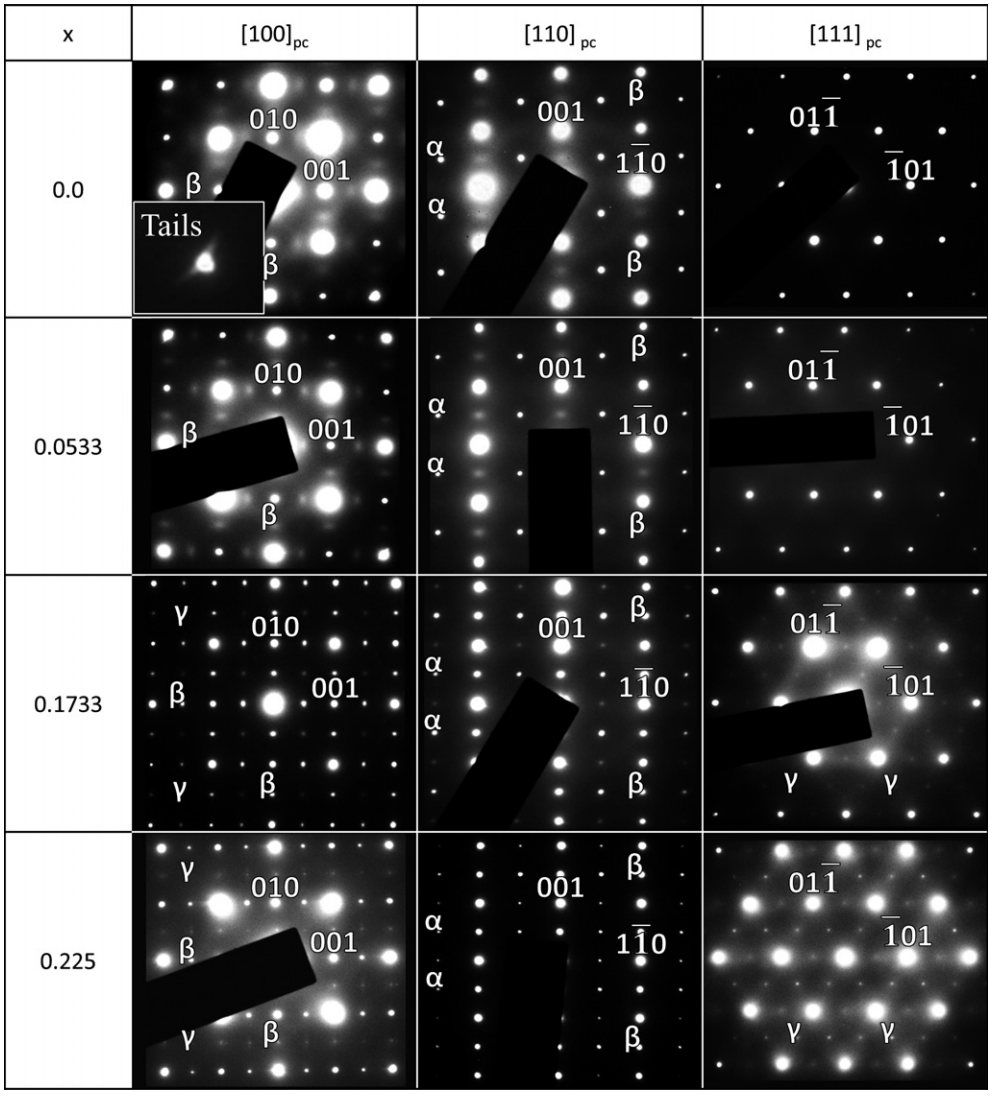

FIGURE 5 $Na_{(1-3x)/2}La_{(1+x)/2}TiO_3$ selected area electron-diffraction patterns of x=0.0-0.225 with the associated pseudo-cubic indexing. Some of the α, β, and γ superlattice reflections are represented for each pattern

expect further from the 1:1 stoichiometry (even though that order is only short-range at x=0).

Figure 5 shows selected-area electron-diffraction patterns (SADPs) of $Na_{(1-3x)/2}La_{(1+x)/2}TiO_3$ indexed according to the pseudocubic cell; whereas Figure 6 shows the same SADPs calculated and indexed according to the actual reported structures. TEM results showed two sets of superlattice reflections, (ie, superlattices from A-site ordering, β, and in-phase octahedral tilting, γ) in the $[100]_{pc}$ zone axis for x≥0.0533, but a single diffuse set at x=0 corresponding only to short-range ordering. The β superlattice reflections observed in the x=0 composition are not only diffuse, indicative of short-range order, but are also slightly curved (inset), suggestive of the existence of ordered nanodomains for which the Bragg condition is relaxed. Diffraction from such nanodomains occurs at a wider angular range than would otherwise be expected, in an analogous way to peak broadening observed in XRD patterns and explained via the Scherrer formula, but the spacing of crystalline planes within the domains remains constant; thus diffraction arcs are observed in SADPs. Two sets of superlattice reflections also appeared in the $[110]_{pc}$ zone patterns (Figure 5) due to A-site ordering (β) and anti-phase octahedral tilting (α); but while the latter are always discreet spots, the ordering reflections are again diffuse for x=0 and only discrete for x≥0.0533. The symbols α, β, and γ correspond to ½{odd, odd, odd}, ½{even, even, odd}, and ½{odd, odd, even}, respectively.

Beta reflections have typically been ascribed to antiparallel cation displacements; however, the superlattice peaks

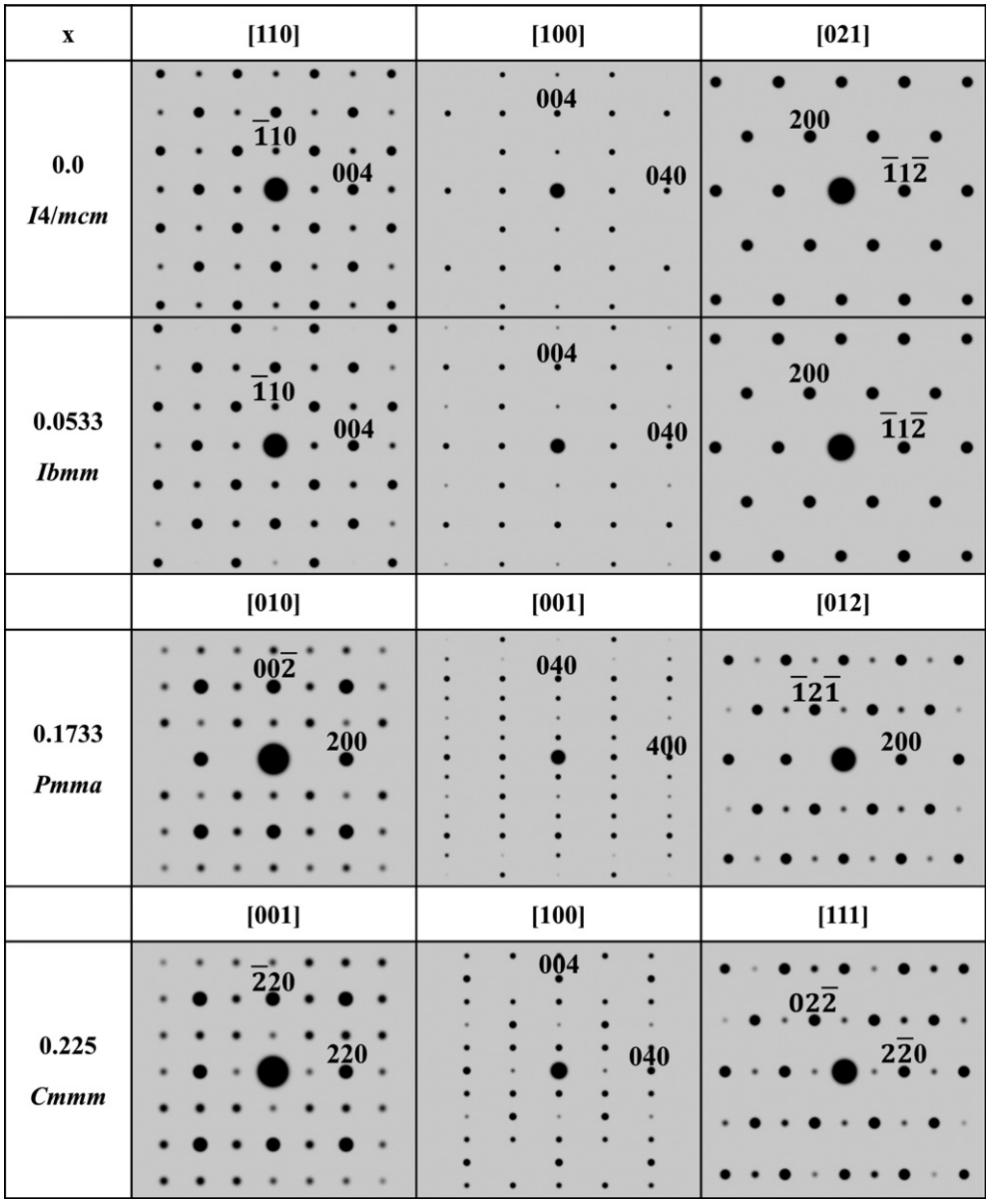

FIGURE 6 $Na_{(1-3x)/2}La_{(1+x)/2}TiO_3$ selected area electron-diffraction patterns of x=0.0-0.225 with the appropriate space group indexing

observed in Figure 2 correspond to those in the top left-hand side pattern of Figure 3 (ie, ordering and not cation displacement). Furthermore, ordering is the only explanation for the observed ½(010) peak at 11.39° in Figure 3 or, by extension, the ½{010} diffuse spots in Figure 5. Antiparallel cation displacements can be discounted due to the lack of a strong ½(111) reflection, and parallel displacement can similarly be ruled out due to the lack of a strong ½(101) reflection (Figure 3). Diffuse scattering such as that observed in Figure 5 is commonly attributed to short-range ordering effects but can also arise due to spinodal decomposition or premartensitic reactions,[61] neither of which is expected in this system. Indeed, such diffuse scattering is normally attributed to short-range ordering phenomena in both pyrochlores[42] and NaCl-structured transition-metal carbides/nitrides[62] as well as other systems.[63]

In Figure 5 it is noteworthy that the $[111]_{pc}$ patterns for x=0.1733 and x=0.225 both contain three sets of weak γ superlattice reflections, whereas the corresponding calculated patterns in Figure 6 contain just a single set each. The extra two sets of reflections could be explained by overlapping twin variants;[44] however, as care was taken to avoid this potential complication and every $<111>_{pc}$ pattern observed in both compositions contained similar reflections, it seems more likely that the models in *Pmma*[9] or *Cmmm* (reported for x=0.2233)[9] cannot fully explain this structure.

A fast Fourier transform mask was applied to high-resolution (HR-TEM) images in the $[100]_{pc}$ zone axis (Figure 7) to show the difference between the fundamental structure and the superstructure. Twinning is also apparent in Figure 7 at x=0.

As an additional example, the well-studied ion-conductor $(Li_{0.5}La_{0.5})TiO_3$ can be considered. Because its ideal A-site size is so small, r_A=1.3059 Å, this composition falls outside the existing range of the empirical model (1.34 Å≤r_A≤1.61 Å); however, the negative errors for a'_{pc} suggested cation ordering on the A site causing a volume expansion, or to be more precise, a stretching of the average A–O bond length (Figure 8). In this case the $Li_{(1-3x)/2}La_{(1+x)/2}TiO_3$ (LLT) x=0 composition has been reported with long-range A-site order. Increasing the r_A for x=0 by just 0.072 Å is sufficient to reduce the error in a'_{pc} to 0.00%. As is the case for NLT, the degree of cation order in LLT decreases with increasing x even as the degree of vacancy ordering increases (Figure 8). Table 8 verifies via DFT calculations that that the unit volume of $Li_{0.5}La_{0.5}TiO_3$ increases upon layered A-site ordering.

As yet another example, the superconductor $(Na_{0.5}La_{0.5})(Mg_{0.5}W_{0.5})O_3$ (NLMW) is an oxide perovskite that has

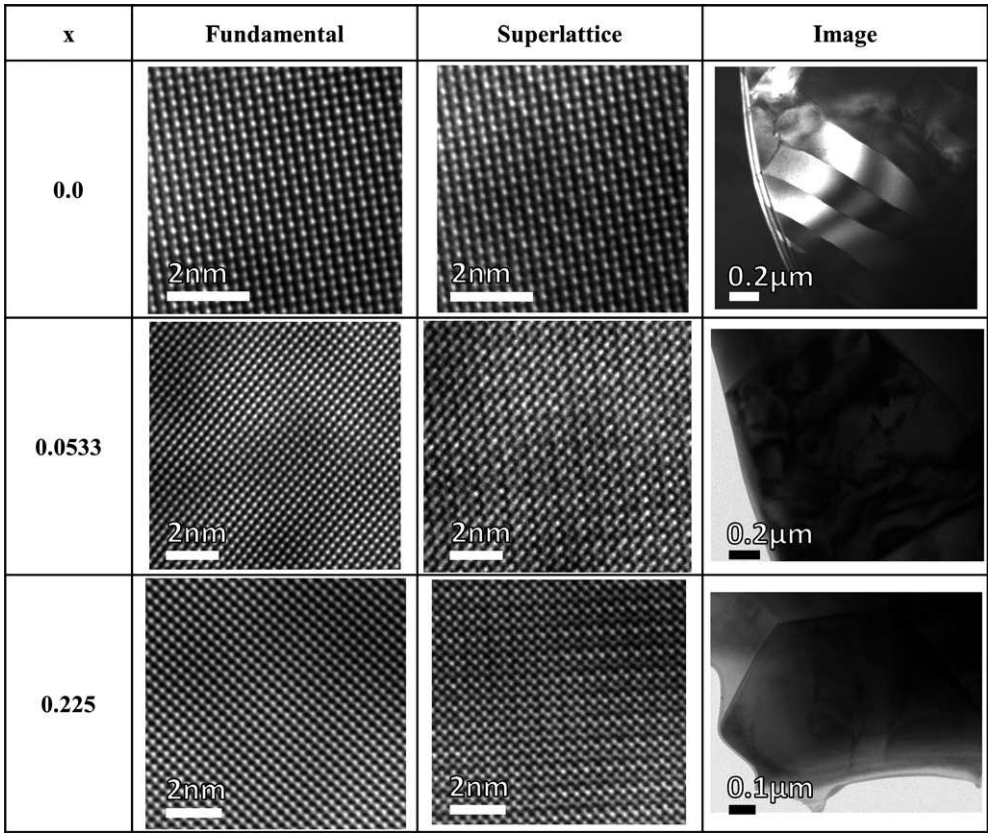

FIGURE 7 $Na_{(1-3x)/2}La_{(1+x)/2}TiO_3$ selected transmission electron microscopy images using a reflections mask and inverse-fast Fourier transform to show the difference between the fundamental and superlattice reflections

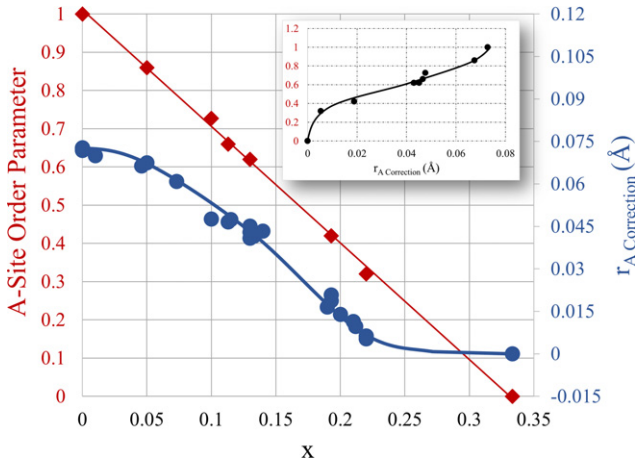

FIGURE 8 $Li_{(1-3x)/2}La_{(1+x)/2}TiO_3$ order parameter and $r_{A\ correction}$ (Å) where both are functions of x. Ordering from reported site-occupancy numbers.[49-60,65-67] Inset shows the order parameter as a function of $r_{A\ correction}$ (Å) and can be thought of as an empirical model for ordering (0=disorder, 1=fully ordered) [Color figure can be viewed at wileyonlinelibrary.com]

the same A-site species as NLT; however, NLMW has been reported[64] with long-range cation ordering on both the A and B sites. As reported previously,[30] the model suggests that the B site contracts upon ordering while the A site expands. Initially, NLMW calculations show a'_{pc}=3.9762 Å and a''_{pc}=3.9727 Å, resulting in errors of 1.294 84% and 1.204 27%, respectively. Using an iterative process to determine the A- and B-site sizes which minimize both errors, it was found that r_B decreases by 0.026 793 Å (to r_B=0.633 21 Å) while r_A simultaneously increases in size by 0.005 849 Å (to r_A=1.380 85 Å). The final error in both a'_{pc} and a''_{pc} is 0.0000%. For the composition $(Na_{0.3333}La_{0.5556})(Mg_{0.5}W_{0.5})O_3$, the model predicts an A-site size increase of about 0.013 36 Å (to r_A=1.232 25 Å)—a lower value indicative of the lower degree of cation ordering expected further from the 1:1 stoichiometry. In the case of $(K_{0.5}La_{0.5})(Mg_{0.5}W_{0.5})O_3$ (KLMW), which has the same B-site species as NLMW, both the A-site and B-site cations are also ordered.[64] The model also shows that the B site contracts and the A site grows upon ordering. Initially, KLMW calculations show a'_{pc}=4.0533 Å and a''_{pc}=4.0822 Å, resulting in errors of 2.538 74% and 3.271 63%, respectively. Again using an iterative process to determine the correct A- and B-site sizes, it was found that the B-site size decreases by 0.104 757 Å (to r_B=0.555 24 Å) and the A-site size increases by 0.073 501 Å (to r_A=1.5735Å), which results in errors of 0.0000% for both a'_{pc} and a''_{pc}. In addition, the model shows that for $(K_{0.3333}La_{0.5556})(Mg_{0.5}W_{0.5})O_3$ the A-site size increase is only 0.052 644 Å—again less than that at x=0, indicative of the lower degree of cation order as x increases. These results are summarized in Table 9.

4 | CONCLUSIONS

Four samples in the $Na_{(1-3x)/2}La_{(1+x)/2}TiO_3$ system (x=0, 0.0533, 0.1733 and 0.225) were synthesized using a conventional solid-state mixed-oxide method. The short-range ordered structure of $Na_{0.5}La_{0.5}TiO_3$ was observed via electron diffraction and predicted via an empirical model, which also suggests a volume increase upon ordering. Even though thermodynamics dictates that a finite concentration of intrinsic vacancies exists even at x=0, there can be no 1:1 long-range vacancy ordering at this or other low-x compositions where the presence of vacancies is nonstoichiometric. First-principles calculations using DFT support these conclusions. $Na_{(1-3x)/2}La_{(1+x)/2}TiO_3$ perovskites have an A-site ordered layered structure, and the degree of cation order decreases as x increases. Similar A-site ordering and volume expansion has been observed in $Li_{(1-3x)/2}La_{(1+x)/2}TiO_3$ and in both $(Na_{0.5}La_{0.5})(Mg_{0.5}W_{0.5})O_3$ and $(K_{0.5}La_{0.5})(Mg_{0.5}W_{0.5})O_3$. The implication of this empirical modeling method is that it may be possible to predict the degree of cation ordering in complex perovskite systems.

ACKNOWLEDGMENTS

This work has been supported by the National Science Foundation (DMR-1052788) and the Micron School of Materials Science and Engineering at Boise State University. The authors are grateful to Dr. Karthik Chinnathambi of the Boise State Center for Materials Characterization (BSCMC). Computing facilities were provided by Boise State University's R1 cluster and Idaho National Laboratory's high performance computing (HPC) center.

REFERENCES

1. Miller V, Tidrow S. Perovskites: Temperature and coordination dependent ionic radii. *Integrated Ferroelectrics*. 2013;148:1–16.
2. Sun P, Nakamura T, Shan Y, Inaguma Y, Itoh M. High temperature quantum paraelectricity in perovskite-type titanates $Ln_{(1/2)}Na_{(1/2)}TiO_{(3)}$ (Ln = La, Pr, Nd, Sm, Eu, Gd and Tb). *Ferroelectrics*. 1997;200:93–107.
3. Muller K, Burkard H. $SrTiO_3$—Intrinsic quantum para-electric below 4-K. *Phys Rev B*. 1979;19:3593–3602.
4. Brous J, Fankuchen I, Banks E. Rare earth titianates with a perovskite structure. *Acta Crystallogr A*. 1953;6:67–70.
5. Agranovskaya A. Physical-chemical investigation of the formation of complex ferroelectrics with perovskite structure. *Izvestiya Akademii Nauk SSR, Seriya Fizicheskaya*. 1960;24:1275–1281.
6. Miao J, Li L, Liu H, et al. Structure characteristics and valence state study for $La_{1-x}Na_xTiO_3$ synthesized under high-pressure and high-temperature conditions. *Mater Lett*. 2000;42:1–6.
7. Mitchell R, Chakhmouradian A. A structural study of the perovskite series $Na_{1/2+x}La_{1/2-3x}Th_{2x}TiO_3$. *J Solid State Chem*. 1998;138:307–312.
8. Ruiz A, Lopez M, Pico C, Veiga M. New $La_{2/3}TiO_3$ derivatives: Structure and impedance spectroscopy. *J Solid State Chem*. 2002;163:472–478.
9. Ruiz A, Lopez M, Pico C, Veiga M. Structural modifications induced by composition in the $La_{1.33-x}Na_{3x}Ti_2O_6$ perovskites: A neutron diffraction study. *Chem Mater*. 2005;17:1391–1397.

10. Li Y, Qin S, Seifert F. Phase transitions in A-site substituted perovskite compounds: The $(Ca_{1-2x}Na_xLa_x)TiO_3$ (0 x 0.5) solid solution. *J Solid State Chem*. 2007;180:824–833.
11. Ranjan R, Senyshyn A, Boysen H, Baehtz C, Frey F. Crystal structures of $Na_{(1/2)}Ln_{(1/2)}TiO_{(3)}$ (Ln: La, Eu, Tb). *J Solid State Chem*. 2007;180:995–1001.
12. Garg R, Senyshyn A, Boysen H, Ranjan R. Structure and phase transition of $Na_{(0.5)}La_{(0.5)}TiO_{(3)}$. *Journal of Physics-Condensed Matter*. 2008;20:1–6.
13. Knapp M, Woodward P. A-site cation ordering in $AA'BB'O_6$ perovskites. *J Solid State Chem*. 2006;179:1076–1085.
14. Inaguma Y, Tsuchiya T, Katsumata T. Systematic study of photoluminescence upon band gap excitation in perovskite-type titanates $R_{1/2}Na_{1/2}TiO_3$: Pr (R = La, Gd, Lu, and Y). *J Solid State Chem*. 2007;180:1678–1685.
15. Jimenez R, Rivera A, Varez A, Sanz J. Li mobility in $Li_{0.5-x}Na_xLa_{0.5}TiO_3$ perovskites (0 × 0.5) Influence of structural and compositional parameters. *Solid State Ionics*. 2009;180:1362–1371.
16. Harunsani M, Woodward D, Peel M, Ashbrook S, Walton R. Investigation of the hydrothermal crystallisation of the perovskite solid solution $NaCe_{1-x}La_xTi_2O_6$ and its defect chemistry. *J Solid State Chem*. 2013;207:117–125.
17. García-Martína S, Urones-Garrote E, Knapp MC, King G, Woodward PM. Structural complexity in $AA'MM'O_6$ perovskites. A transmission electron microscopy study. *Mater Res Soc Symp Proc*. 2009;1148:15–05.
18. Howard C, Zhang Z. Structures and phase transition in the layered perovskite $La_{0.6}Sr_{0.1}TiO_3$: A new orthorhombic structure solved from high-resolution diffraction in combination with group theoretical analysis. *J Phys-Condens Matter*. 2003;15:4543–4553.
19. Gönen Z, Paluchowski D, Zavalij P, Eichhorn B, Gopalakrishnan J. Reversible cation/anion extraction from $K_2La_2Ti_3O_{10}$: Formation of new layered titanates, $KLa_2Ti_3O_{9.5}$ and $La_2Ti_3O_9$. *Inorg Chem*. 2006;45:8736–8742.
20. Richard M, Brohan L, Tournoux M. Synthesis, characterization, and acid exchange of the layered perovskites—$A_2Nd_2Ti_3O_{10}$ (A=NA, K). *J Solid State Chem*. 1994;112:345–354.
21. Sekiya T, Yamamoto T, Torii Y. Cation ordering in $(NaLa)(MgW)O_6$ with the perovskite structure. *Bull Chem Soc Jpn*. 1984;57:1859–1862.
22. Leinenweber K, Parise J. High-pressure synthesis and crystal-structure of $CaFeTi_2O_6$, a new perovskite structure type. *J Solid State Chem*. 1995;114:277–281.
23. Ducau M, Suh K, Senegas J, Darriet J. Crystal-structure and NMR-studies of a cubic perovskite—The fluoride $NaBaLiNiF_6$. *Mater Res Bull*. 1992;27:1115–1123.
24. Deschanvres A, Raveau B, Tollemer F. Substitution of copper for a bivalent metal in titanates of perovskite type. *Bull Soc Chim Fr*. 1967;11:4077–4078.
25. Propach V. Kristallstruktur von $Ca_{0.5}Cu_{1.5}Ti_2O_6$, $Cu_{1.5}TaTiO_6$ und $CuTa_2O_6$. Das spektroskopische Verhalten von Cu^{2+}-Ionen in kuboktaedrischer Umgebung. Zeitschrift für Anorganische und Allgemeine. *Chemie*. 1977;435:161–171.
26. Glazer AM. The classification of tilted octahedra in perovskites. *Acta Crystallogr Sect B*. 1972;28:3384–3392.
27. Ubic R, Subodh G, Sebastian M, Gout D, Proffen T. Structure of compounds in the $Sr_{1-3x/2}Ce_xTiO_3$ homologous series. *Chem Mater*. 2008;20:3127–3133.
28. Ubic R, Subodh G, Gout D, Sebastian M, Proffen T. Crystal structure of $Sr_{0.4}Ce_{0.4}TiO_3$ ceramics. *Chem Mater*. 2009;21:4706–4710.
29. Ubic R, Tolman K, Chan K, Lundy N, Letourneau S, Kriven W. Effective size of vacancies in aliovalently doped $SrTiO_3$ perovskites. *J Alloy Compd*. 2013;575:239–245.
30. Ubic R, Tolman K, Talley K, et al. Lattice-constant prediction and effect of vacancies in aliovalently doped perovskites. *J Alloy Compd*. 2015;644:982–995.
31. Shannon R. Revised effective ionic-radii and systematic studies of interatomic distances in halides and chalcogenides. *Acta Crystallogr Sec A*. 1976;32:751–767.
32. Goldschmidt V. The laws of crystal chemistry. *Naturwissenschaften*. 1926;14:477–485.
33. Ubic R. Revised method for the prediction of lattice constants in cubic and pseudocubic perovskites. *J Am Ceram Soc*. 2007;90:3326–3330.
34. Tolman K, Ubic R, Papac M, et al. Structural effect of aliovalent doping in lead perovskites. *J Solid State Chem*. 2015;225:359–367.
35. Finger L, Cox D, Jephcoat A. A correction for powder diffraction peak asymmetry due to axial divergence. *J Appl Crystallogr*. 1994;27:892–900.
36. Kresse G, Furthmuller J. Efficient iterative schemes for ab initio total-energy calculations using a plane-wave basis set. *Phys Rev B*. 1996;54:11169–11186.
37. Perdew J, Burke K, Ernzerhof M. Generalized gradient approximation made simple. *Phys Rev Lett*. 1996;77:3865–3868.
38. Blöchl P. Projector augmented-wave method. *Phys Rev B*. 1994;50:17953–17979.
39. Kresse G, Joubert D. From ultrasoft pseudopotentials to the projector augmented-wave method. *Phys Rev B*. 1999;59:1758–1775.
40. Askeland DR. *The Science and Engineering of Materials*. Boston, MA: PWS-Kent Pub. Co.; 1989.
41. Zhang Z, Middleburgh SC, De Los Reyes M, et al. Gradual structural evolution from pyrochlore to defect-fluorite in $Y_2Sn_{2-x}Zr_xO_7$: Average vs local structure. *J Phys Chem C*. 2013;117:26740–26749.
42. Karthik C, Anderson T, Gout D, Ubic R. Transmission electron microscopic study of pyrochlore to defect-fluorite transition in rare-earth pyrohafnates. *J Solid State Chem*. 2012;194:168–172.
43. Mani R, Bhuvanesh N, Ramanujachary K, Green W, Lofland S, Gopalakrishnan J. A novel one-pot metathesis route for the synthesis of double perovskites, $Ba_3MM'2O_9$ (M = Mg, Ni, Zn; M '= Nb, Ta) with 1:2 ordering of M and M′ atoms. *J Mater Chem*. 2007;17:1589–1592.
44. Ubic R, Hu Y, Abrahams I. Neutron and electron diffraction studies of La $(Zn_{1/2}Ti_{1/2})O_3$ perovskite. *Acta Crystallogr Sec B-Struc Sci*. 2006;62:521–529.
45. Yang J, Choo W, Lee C. Ca_2MgWO_6 from neutron and X-ray powder data. *Acta Crystallogr Sec C-Crystal Struc Commun*. 2003;59:I86–I88.
46. Mishra A, Poswal H, Acharya S, Tyagi A, Sharma S. Structural evolution of double perovskite $Sr_{(2)}MgWO_{(6)}$ under high pressure. *Phys Status Solidi B-Basic Solid State Phys*. 2010;247:1773–1777.
47. Day B, Bley N, Jones H, et al. Structures of ordered tungsten- or molybdenum-containing quaternary perovskite oxides. *J Solid State Chem*. 2012;185:107–116.
48. Baldinozzi G, Sciau P, Pinot M, Grebille D. Crystal-structure of the antiferroelectric perovskite Pb_2MgWO_6. *Acta Crystallogr Section B-Struc Sci*. 1995;51:668–673.
49. Alonso J, Sanz J, Santamaria J, Leon C, Varez A, Fernandez-Diaz M. On the location of Li^+ cations in the fast Li cation conductor $La_{0.5}Li_{0.5}TiO_3$ perovskite. *Angewandte Chemie-International Edition*. 2000;39:619.
50. Alonso JA, Ibarra J, Paris MA, et al. Relationship between crystal structure and Li^+-conductivity in $La_{0.5}Li_{0.5}TiO_3$ perovskite. *Mater Res Soc Symposia Proc*. 2000;575:337–342.
51. Ibarra J, Varez A, Leon C, Santamaria J, Torres-Martinez L, Sanz J. Influence of composition on the structure and conductivity of the fast ionic conductors $La_{2/3-x}Li_{3x}TiO_3$ (0.03 × 0.167). *Solid State Ionics*. 2000;134:219–228.
52. Kang E-T, Kwon Y-J. The structure determination of $La_{2/3-x}Li_{3x\ 1/3-2x}TiO_3$ by the powder neutron and X-ray diffraction. *J Korean Ceram Soc*. 2003;40:513–518.
53. Ruiz A, Lopez M, Veiga M, Pico C. Electrical properties of $La_{1.33-x}Li_{3x}$-Ti_2O_6 (0.1<x<0.3). *Solid State Ionics*. 1998;112:291–297.
54. Inaguma Y, Katsumata T, Itoh M, Morii Y, Tsurui T. Structural investigations of migration pathways in lithium ion-conducting $La_{2/3-x}Li_{3x}TiO_3$ perovskites. *Solid State Ionics*. 2006;177:3037–3044.
55. Fourquet J, Duroy H, CrosnierLopez M. Structural and microstructural studies of the series $La_{2/3-x}Li_{3x}$ $V_{1/3-2x}TiO_3$. *J Solid State Chem*. 1996;127:283–294.

56. Cheng Y, Bi Z, Huq A, et al. An integrated approach for structural characterization of complex solid state electrolytes: The case of lithium lanthanum titanate. *J Mater Chem A*. 2014;2:2418–2426.
57. Ruiz A, Lopez M, Veiga M, Pico C. Structural refinement by neutron diffraction of $La_{1.12}Li_{0.62}Ti_2O_6$. *J Solid State Chem*. 1999;148:329–332.
58. Kishida K, Miyata M, Wada N, et al. Crystal and defect structures of $La_{2/3-x}Li_{3x}TiO_3$ (x similar to 0.1) produced by a melt process. *J Electron Microsc*. 2007;56:225–234.
59. Bhuvanesh N, Bohnke O, Duroy H, Crosnier-Lopez M, Emery J, Fourquet J. Topotactic H^+/Li^+ ion exchange on $La_{2/3-x}Li_{3x}TiO_3$: New metastable perovskite phases $La_{2/3-x}TiO_{3-3x}(OH)_{(3x)}$ and $La_{2/3-x}TiO_{3-3x/2}$ obtained by further dehydration. *Mater Res Bull*. 1998;33:1681–1691.
60. Sanz J, Varez A, Alonso J, Fernandez M. Structural changes produced during heating of the fast ion conductor $Li_{0.18}La_{0.61}TiO_3$. A neutron diffraction study. *J Solid State Chem*. 2004;177:1157–1164.
61. Loretto MH. *Electron Beam Analysis of Materials*. London; New York: Chapman and Hall; 1984.
62. Sauvage M, Parthé E. Vacancy short-range order in substoichiometric transition metal carbides and nitrides with the NaCl structure. II. Numerical calculation of vacancy arrangement. *AYA Acta Crystallogr Sec A*. 1972;28:607–616.
63. Williams DB, Carter CB. *Transmission Electron Microscopy: A Textbook For Materials Science*. New York, NY: Springer; 2009.
64. Arillo M, Gomez J, Lopez M, Pico C, Veiga M. Structural and electrical characterization of new materials with perovskite structure. *Solid State Ionics*. 1997;95:241–248.
65. Sommariva M, Catti M. Neutron diffraction study of quenched $Li_{0.3}La_{0.567}TiO_3$ lithium ion conducting perovskite. *Chem Mater*. 2006;18:2411–2417.
66. Inaguma Y, Katsumata T, Itoh M, Morii Y. Crystal structure of a lithium ion-conducting perovskite $La_{2/3-x}Li_{3x}TiO_3$ (x=0.05). *J Solid State Chem*. 2002;166:67–72.
67. Yashima M, Ishimura D, Ohoyama K. Temperature dependence of lattice parameters and anisotropic thermal expansion of bismuth oxide. *J Am Ceram Soc*. 2005;88:2332–2335.

How to cite this article: Tolman K, Ubic R, Liu B, et al. Empirical evidence for A-site order in perovskites. *J Am Ceram Soc*. 2017;100:429–442. doi:10.1111/jace.14547.